**Blaž Vajda, Zoran Žunič, Želimir Dobovišek, Breda Kegl**

ISSN 0350-350X
GOMABN 50, 4, 335-360
Stručni rad/Professional paper
UDK 532.51 : .001.575 : .001.572 : 518.5 : 516.3 : 532.525 : 532.528

# UTJECAJ RAZLIČITIH TIPOVA MREŽE NA PROCES KAVITACIJE U OTVORU SAPNICE BRIZGALJKE

*Sažetak*

*Isparivost dizelskog goriva u otvoru mlaznice u velikoj mjeri utječe na značajke ubrizgavanja i formiranja mlaza. U radu se analizira utjecaj različitih tipova mreže na procese kavitacije. Budućid da je CPU (Centralna Procesorska Jedinica) vremena često dugačka, u analizi su korišteni parcijalni modeli. Numeričku analizu izvodili smo za dvije vrste tekućina, dizel (D2) i biodizel (B100), koristeći računski program FIRE za dinamiku fluida (CFD). Rezultati su uspoređivani za razne tipove mreže za obje vrste goriva i pokazuju da veće razlike u tlaku uzrokuju veću kavitaciju u otvoru sapnice brizgaljke te ističu važnost strukture i gustoće mreže.*

## Uvod

Razvoj suvremenih dizelovih motora uglavnom je usmjeren na podizanje tlaka ubrizgavanja i na mogućnosti ubrizgavanja nekoliko mlazova tijekom pojedinačnog ciklusa. Obje preinake pozitivno utječu na značajke motora i na procese nastanka emisije. Nasuprot tome, podizanje tlaka ubrizgavanja uvjetuje veće brzine protoka u kanalima i isparavanje goriva u provrtima sapnice. Gorivo isparava na oštrim ivicama na ulasku u sapnicu, gdje tlak padne ispod tlaka isparavanja goriva. Para se širi duž provrta sapnice i može tako prispjeti do izlaza. Isparivost goriva i kavitacijski proces u otvoru sapnice značajno utječu na tok unutar sapnice, proces formiranja mlaza, a može uzrokovati eroziju materijala sapnice, kada dolazi do kolapsa mjehura u blizini stijenke sapnice. Budući da je promjer sapnice brizgaljke obično manji od 1 mm, a razlika tlaka može prelaziti 200 MPa, eksperimentalne analize su prilično teške i ograničene. Tako se većina eksperimentalnih analiza dvofaznog toka u sapnici brizgaljke odnosi na mjerenja i motrenja na uvećanim modelima.

Nasuprot tome, računalni paketi na temelju dinamike fluida, CFD, u posljednje vrijeme postaju sve značajniji, budući da se uporabom trodimenzionalne analize može izračunati velik broj parametara u svakoj pojedinačnoj ćeliji modela sapnice. Osnovni problem koji se javlja kod CFD analize je potrebno vrijeme računanja. Da bi se skratilo vrijeme potrebno za računanje pojedinačne analize, koriste se pojednostavljeni modeli sapnice.

## Geometrija sapnice

Napravljene su analize za sapnicu s jednim provrtom s mrtvom zapreminom i oštrim ivicama na ulaznom dijelu. Dimenzije ispitivane sapnice su sažete u tablici 1.

Tablica 1: Dimenzije sapnice

| | |
|---|---|
| Promjer provrta sapnice | 0,68 mm |
| Dužina kanala provrta | 1 mm |
| Promjer komore mrtvog volumena | 1,5 mm |
| Promjer sjedišta igle | 1,36 |
| Kut konusa vrha igle | 120° |
| Kut konusa sjedišta igle | 60° |
| Maksimalni hod igle | 0,30 mm |

## Numerički model

### Teorijske osnove

Numeričke analize su izvođene CFD programom FIRE. Dvofazni tok se računa dvojednadžbenim modelom, pri čemu se tekućina smatra kontinuiranom, a parna faza disperzivnom (raspoređenom).

Jednadžba očuvanja mase:

$$\frac{\partial \alpha_k \rho_k}{\partial t} + \nabla \cdot \rho_k \mathbf{v}_k = \sum_{l=1;l\neq k}^{N} \Gamma_{kl} \tag{1}$$

$\alpha_k$ je volumenski dio faze k, $v_k$ je brzina faze k, a $\Gamma_{kl}$ predstavlja prijenos mase između obje faze. Uvjet sukladnosti mora biti očuvan:

$$\sum_{k=1}^{N} \alpha_k \tag{2}$$

Jednadžba očuvanja količine gibanja je:

$$\frac{\partial \alpha_k \rho_k \mathbf{v}_k}{\partial t} + \nabla \cdot \rho_k \mathbf{v}_k \mathbf{v}_k = -\alpha_k \nabla p + \nabla \alpha_k \left(\tau_k + T_k^{'}\right) + \alpha_k \rho_k \mathbf{g} + \sum_{l=1;l\neq k}^{N} \mathbf{M}_{kl} + \mathbf{v}_k \sum_{l=1;l\neq k}^{N} \Gamma_{kl} \tag{3}$$

pri čemu je *f* vektor volumenske sile, koja uključuje gravitaciju *g*; $M_{kl}$ predstavlja količinu gibanja koja je posljedica gibanja međusobnog djelovanja faza k i l, a *p* predstavlja tlak. Pretpostavlja se, da je tlak jednak u svim fazama, pri čemu je $\tau_k$ napetost smicanja faze k, a označava se na sljedeći način:

$$\tau_k = \mu_k \left[ \left( \nabla v_k + \nabla v_k^t \right) - \frac{2}{3} \nabla \cdot v_k \right] \tag{4}$$

gdje je $\mu_k$ molekularna viskoznost.

Reynoldsov napon $T_{kt}$ je jednak:

$$T_k^{'} = -\rho_k \overline{\nabla v_k^{'} v_k^{'}} = \mu_k^{'}\left[\left(\nabla v_k + \nabla v_k^t\right) - \frac{2}{3}\nabla \cdot v_k\right] - \frac{2}{3}\nabla \cdot v_k I \tag{5}$$

Turbulentna viskoznost je modelirana kao:

$$\mu_k^{'} = \rho_k C_\mu \frac{k_k^2}{\varepsilon_k} \tag{6}$$

S obzirom da su analize predstavljene u ovom prilogu izvedene kod konstantne temperature, jednadžbe za očuvanje entalpije neće se detaljnije predstavljati.
Jednadžba za očuvanje turbulentne kinetičke energije:

$$\begin{aligned}&\frac{\partial \alpha_k \rho_k k_k}{\partial t} + \nabla \cdot \alpha_k \rho_k \mathbf{v}_k k_k = \\ &\nabla \cdot \alpha_k \left(\mu_k + \frac{\mu_k^{'}}{\sigma_k}\right)\nabla k_k + \alpha_k P_k + \alpha_k P_{B,k} - \alpha_k \rho_k \varepsilon_k + \sum_{l=1;l\neq k}^{N} K_{kl} + k_k \sum_{l=1;l\neq k}^{N} \Gamma_{kl}\end{aligned} \tag{7}$$

Jednadžba za turbulentnu disipaciju:

$$\begin{aligned}&\frac{\partial \alpha_k \rho_k \varepsilon_k}{\partial t} + \nabla \cdot \rho_k \mathbf{v}_k \varepsilon_k = \nabla \cdot \alpha_k \left(\mu_k + \frac{\mu_k^{'}}{\sigma_\varepsilon}\right)\nabla \varepsilon_k + \alpha_k C_1 P_k \frac{\varepsilon_k}{k_k} - \alpha_k C_2 \rho_k \frac{{}_k \varepsilon_k^2}{k_k} \\ &+ \alpha_k C_3 \max\left(P_{B,k}, 0\right)\frac{\varepsilon_k}{k_k} - \alpha_k C_4 \rho_k \varepsilon_k \nabla \cdot \mathbf{v}_k + \sum_{l=1;l\neq k}^{N} D_{kl} + \varepsilon_k \sum_{l=1;l\neq k}^{N} \Gamma_{kl}\end{aligned} \tag{8}$$

U dvojednadžbeni model mogu se uključiti brojni članovi za prijenos mase (s obzirom na vrstu dvofaznog toka). U predstavljenoj analizi upotrijebili smo kavitacijski model. Član za prijenos mase je definiran sljedećim jednadžbama:

$$\Gamma_c = \frac{1}{C_R}\sin g(\Delta p) \cdot 3{,}85 \cdot \frac{\rho_d}{\sqrt{\rho_c}} N^{'''1/3} \alpha_d^{2/3} \left|\Delta p\right|^{1/2} \tag{9}$$

$$\Gamma_d = \sin g(\Delta p) \cdot 3{,}85 \cdot \frac{\rho_d}{\sqrt{\rho_c}} N^{'''1/3} \alpha_d^{2/3} \left|\Delta p\right|^{1/2} \tag{10}$$

Pri čemu efektivna razlika tlaka iznosi:

$$\Delta p = p_{sat} - (p - C_E \frac{2}{3}\rho_c k_c) \tag{11}$$

$C_E$ je Eglerjev koeficijent koji mijenja vrijednosti između 1 i 1,4. $C_{cr}$ je faktor koji prigušuje kondenzaciju. $N'''$ je brojčana gustoća mjehurića, koja se izračuna pomoću linearne aproksimacije s negativnim k:

$$N''' = \begin{cases} N_0''' & \alpha_d \le 0{,}5 \\ 2(N_0''') & \alpha_d > 0{,}5 \end{cases} \tag{12}$$

pri čemu $N_0'''$ predstavlja početnu vrijednost numeričke gustoće mjehurića.
Članak koji bilježi prijenos količine gibanja među fazama je definiran s:

$$M_C = C_D \frac{1}{8} \rho_C A_i''' |v_r| v_r + C_{TD} \rho_c k_c \nabla \alpha_d = -M_d \tag{13}$$

pri čemu je $v_r$ relativna brzina i $A_i'''$ međufazna gustoća tih mjehurića:

$$A_i''' = \pi D_b^2 N''' = (36\pi)^{1/3} \alpha_d^{2/3} \tag{14}$$

$C_D$ je koeficijent, koji predstavlja smanjivanje veličine kapljica:

$$C_D = \begin{cases} \frac{24}{\mathrm{Re}_d} \cdot \left(1 + 0{,}15\,\mathrm{Re}_d^{0{,}687}\right) \Leftarrow \mathrm{Re}_d < 10^3 \\ 0{,}44 \Leftarrow \mathrm{Re}_d \ge 10^3 \end{cases} \tag{15}$$

$C_{TD}$ predstavlja koeficijent turbulentne disipacije, koji iznosi od 0,05 do 0,5.

## Računski model

Za analizu značajke unutarnjeg toka sapnice postoje različiti modeli. Budući da neke analize pokazuju da je značajan pad tlaka samo u području sjedišta igle, mrtvog volumena i provrta sapnice, mreže smo modelirali samo za spometnute dijelove. Za maksimalni hod igle od 0,3 mm, napravili smo dva različita modela sapnice, predstavljajući stvarnu veličinu i polovinu sapnice. Prve analize su pokazale da nema značajnih razlika između rezultata modela za stvarnu veličinu i polovinu mlaznice. Zato smo u daljnjem istraživanju koristili model polovine veličine.

## Početni i granični uvjeti

U skladu s uvjetima koji odgovaraju stacionarnom stanju, specificirani su granični uvjeti na ulazu i izlazu. Korištena goriva u analizi bila su dizelsko gorivo D2 i biodizel B100 s gustoćom 825 kg/m$^3$ za D2 i 875 kg/m$^3$ za B100; temperatura 293,15 K. Dinamička viskoznost je 2,45E-03 Ns/m$^3$ za D2 i 2,65E-03 Ns/m$^3$ za B100. Koristili smo k-ε model. Budući da su maksimalne brzine toka korištenih fluida znatno manje od brzine zvuka, pretpostavili smo, da je fluid nestišnjiv.

### Korišteni tipovi mreže i njihove različite gustoće

Numerička analiza uključuje različite gustoće i tipove mreže. Gustoća i njoj pripadajući tip mreže su predstavljeni u tablici 2 i na slici 1. Standardni pristup uključuje tipove mreže različite blokovne strukture; mi smo imali mogućnost da ih uspoređujemo (po vremenu) po građi s ciljem proučavanja razlike među njima.

Tablica 2: Različite gustoće i pripadajući tipovi mrežice

| Naziv | Broj korištenih elemenata | Tip mrežice | Fizički model |
|---|---|---|---|
| mreža 1 | 21.440 | višeblokovna struktura | Jednofazni |
| mreža 2 | 41.920 | višeblokovna struktura | Jednofazni |
| mreža 3 | 162.050 | višeblokovna struktura | Jednofazni |
| mreža 4 | 22.880 | višeblokovna struktura | Jednofazni |
| mreža 5 | 44.320 | višeblokovna struktura | Jednofazni |
| mreža 6 | 183.040 | višeblokovna struktura | Jednofazni |
| mreža 7 | 254.120 | višeblokovna struktura | Jednofazni |
| mreža 8 | 22.900 | monostruktura | Dvofazni |
| mreža 9 | 42.300 | monostruktura | Dvofazni |
| mreža 10 | 46.540 | monostruktura | Dvofazni |
| mreža 11 | 145.890 | monostruktura | Dvofazni |
| mreža 12 | 175.050 | monostruktura | Dvofazni |
| mreža 13 | 260.550 | monostruktura | Dvofazni |

## Rezultati

Rezultati se odnose na četiri različita mjesta provrta brizgaljke. Mjesta su pokazana na slici 2. Mjesto 1 se nalazi na ulazu, mjesto 2 na izlazu sapnice, a mjesto 3 se nalazi između položaja 1 i 2. Mjesto 4 je uzduž sapnice. Svi rezultati su snimljeni u isto vrijeme (1,765E-03 s). Pretpostavili smo da je u to vrijeme igla u potpuno otvorenomu položaju.

### Rezultati numeričke analize

Profili brzine i podjela obaju dijelova mase koja slijede iz CFD analize različitih modela mreže, predstavljeni su na sljedećim slikama. Slike 3-4 (pogled s lijeva otraga, pogled s desna ispred) pokazuju rezultate razdiobe dijela mase u provrtu sapnice pri različitim gustoćama mreže.

Profil brzine i podjela mase u provrtima sapnice pri različitim gustoćama prikazani na slikama 3-4 približno su identični. Rezultati ukazuju na upravo poznatu činjenicu da je protočna brzina na izlazu veća kod provrta s manjim kutom nagiba, što rezultira u višem protočnom koeficijentu tih provrta. Rezultati numeričke analize profila brzine, relativnog tlaka i dijelova mase mreže blokovne strukture različitih gustoća prikazani su na slikama 6-7 za jednofazni, a na slikama 8-12 za dvofazni tok.

Na slici 5 su prikazani profili brzina za mrežice blokovih tipova strukture jedne faze (B100). Rezultati ne ukazuju na značajne razlike pri različitim gustoćama. Razlike su oko 2 %. Nasuprot tome, ako usporedimo rezultate profila brzina na mjestu 4 (slika 6), razlike su oko 5 %. Ove vrijednosti su manje pri većoj gustoći, od vrijednosti pri manjim gustoćama. Razlog tome je možda u pojavi kavitacije.

Slika 7 prikazuje rezultate relativnog tlaka za jednu fazu (samo B100). Primijetiti se mogu značajne razlike za razne tipove mreže. Za mreže manje gustoće su razlike manje od 0,5 %. U slučaju, da se međusobno uspoređuju rezultati za veće i manje gustoće, razlike iznose oko 10 %.

Profili brzine i raspodjela udjela mase na ulazu u sapnicu gotovo su identični (slike 8, 9 i 10). Usporedba rezultata na slikama 11 do 13 pokazuje kako različiti tipovi mreže značajno utječu na profile brzine. Kada se koristi jednostavna struktura mreže (slika 11), profili brzine su grublji nego u slučaju blokove strukture (slika 13). Kada usporedimo rezultate za razne gustoće mreže, postoje razlike između mreža veće gustoće u odnosu na mreže manje gustoće (slike 5-7 za jednofazni i slike 8-12 za dvofazni model). Rezultati volumenskog udjela predstavljeni su na slici 8. Rezultati za mrežu 1 ukazuju na numerički nedostatak izazvan interpolacijom nedovoljnog broja elementa (vrh na dužini 6,5E-04). Vrhovi na dužini 5,5E-04 za mreže 6 i 7 izazvani su oblakom pare koji se širi kroz provrt, dok ne stigne do izlaza.

Rezultati utjecaja raznih vrsta fluida (D2 i B100) ne ukazuju na značajnu razliku. Polja brzina, profila brzina i distribucija volumenskog udjela na izlazu međusobno su usporedivi. Rezultati se mogu uspoređivati, jer su gustoće korištenih fluida slične i ne razlikuju se mnogo (razlika iznosi oko 50 kg/m$^3$). Razlika dinamičkih viskoznosti je isto tako vrlo mala i nema utjecaja na rezultat. Vrijednosti protoka i dinamičke viskoznosti su se razlikovale (eksperimentalni podaci), dok su, međutim, tlakovi i temperature bile jednake za obje vrste goriva.

Razlike koje pokazuju slike 14-16 su vrlo male. Neke analize udjela mase (indikator kavitacije) su napravljene za razna goriva, i razlike su čak neznatnije i ne mogu se pravilno prikazati kao na slikama 3-4.

Kao što smo već spomenuli, rezultati analize na cijelom i na pola modela sapnice pokazuju značajne razlike. Polja i profili brzina na izlazu i raspodjela tlakova su usporedivi. Ta činjenica je prikazana na slici 17.

Razlika brzine u slučaju mreže 3 – ½ model i mreže 3-model realne dimenzije je najviše 1 % (slika 18). Izračunate vrijednosti koeficijenta proticanja su 0,678 za realna i 0,679 za polovični model, gdje je CPU vremena za polovični model svega 43,5 % od CPU potrebnog pri računanju s modelom realnih dimenzija. Raspodjele tlaka prikazane na slici 18 pokazuju da zona recirkulacije zauzima mali prostor. To znači da je brzina na izlazu veća i isto tako jednolikija. Iz većih brzina na izlazu proizlazi bolja atomizacija (raspršivanje) ubrizganog goriva.

Udjeli pare raznih vrsta fluida su prikazani na slici 19. Struktura kavitacije ne ovisi o dužini provrta sapnice. Oblik kavitacije u početnom dijelu provrta je gotovo identičan. Kasnije se oblak širi kroz provrt dok ne stigne do izlaza.

## Zaključak

Razmatrajući spomenute rezultate, možemo zaključiti slijedeće:

- numerička analiza pokazuje da veće razlike tlaka proizvedu veći opseg kavitacije,
- rezultati numeričke analize pokazuju da je mreža tipa blokovne strukture bolja za numeričke analize provrta sapnice,
- usporedba (obične) strukture i blokovne strukture pokazuje da su profili brzine grublji s običnom strukturom, nego u slučaju kada se koristi blokovna struktura mrežice,
- preporučuje se uporaba mreže veće gustoće (s više od 100 000 elementa) kada se analiziraju tokovi unutar sapnice, ali se mreže manje gustoće (20 000 i 100 000 elementa) isto tako mogu primijeniti za brze procjene,
- rezultati numeričke analize za razne vrste fluida (D2 i B100) su usporedivi, ali se ipak preporučuje da se izvede više simulacija s dodatnim parametrima (tlak, temperatura…),
- prve analize ne pokazuju značajan utjecaj dužine provrta sapnice na oblik kavitacije.

### Literatura

[1] T. Yoda, T. Tsuda, Inflence of injection Nozzle improvement on DI Diesel Engine, SAE paper 970356.
[2] Y. Oishi et al., A computational Study into the Effect of the Injection Nozzle Inclintion Angle on the Flow Characteristics in Nozzle Holes, SAE paper 920580.
[3] C. Arcoumanis et. al., Analysis of the Flow in the Nozzle of a Vertical Multi Hole Diesel Engine Injector, SAE paper 980811.
[4] M. Kato et al., Flow Analysis in Nozzle Hole in Consideration of Cavitation, SAE paper 970052.
[5] Y. Oishi et al., A Computational Study into the Effects of the Injection Nozzle Inclination Angle on the Flow Characteristics in the Nozzle Holes, SAE paper 920580.
[6] K. Melcher, J. Chomiak, Experimentelle Untersuchung der Stroemung durch Dieseleinspritzduesen in stationaer betriebenen Grossmodel, Bosch Techn. Berichte 5 (1976) 4.
[7] ISO-4113:1988, Road Vehicles- Calibration Fluid Diesel Injection Equipment.
[8] H. Hardenberg, Die Nadelhubabhaengigkeit der Durchflussbeiwerte von Lochduessen fuer Direkteinspritzdieselmotoren, MTZ 46 (1985) 4, p. 143-146.
[9] FIRE Version 9 – Users manual, Multiphase Flow, AVL, 2009.
[10] L. C. Ganippa et al., The structure of cavitation and its effect on the spray pattern in a single hole diesel nozzle, SAE paper 2001-01-2008.
[11] L. C. Ganippa et al., Comparison of cavitation phenomena in transparent scaled-up single hole diesel nozzles, 4th International Symposium on Cavitation, California Institute of Technology, Pasadena, 2001.
[12] B. Göschel, Einspritzdüsenverschleiß, Forschungvereinigung Verbrenungskraftmachinen e.V., Heft R245, 1974.
[13] Kavitation. Abschlüßbericht über die Ergebnise des Schwerpunktprogramm 1966-1972, Deutsche Forschungsgemeinschafts, Boppard, 1974.

[14] G. König et al., Analysis of flow and cavitation phenomena in diesel injection nozzles and its effects on spray and mixture formation, 5. Internationales Symposium für Verbrennungsdiagnostik der AVL Deutschland, 6.-7. Juni, Baden Baden, 2002
[15] C. Arcoumanis et al., Visualisation of cavitation in diesel engine injectors, Mec. Ind. (2001) 2, 375-381.
[16] C. Arcoumanis et al., Investigation of cavitation in a vertical multi-hole injector, SAE paper 1999-01-0524.
[17] C. Arcoumanis et al, Cavitation in real-size multi-hole diesel injector nozzles, SAE paper 2000-01-1249.
[18] C. Badock et al, Investigation of cavitation in real size diesel injection nozzle, International Journal of Heat and Fluid Flow 20 (1999).
[19] K. Jung et.al., The breakup characteristics of liquid sheets formed by like-doublet injectors, Journal of Propulsion and Power (sent), http://rpl.snu.ac.kr/.



| UDK | ključne riječi | key words |
|---|---|---|
| 532.51 | numerički model dinamike fluida | computational fluid dynamics CDFmodel |
| .001.575. | gledište ispitivanja na materijalnom modelu | real model investigation viewpoint |
| .001.572 | gledište ispitivanja na teorijskom modelu | theoretical model investigation viewpoint |
| 518.5 | numeričko i grafičko modeliranje procesa | numeric and graphic process modeling |
| 516.3 | mrežni sistem prostornih koordinata | mesh system of space coordinates |
| 532.525 | istjecanje iz sapnica | fluid flow through nozzles |
| 532.528 | kavitacija strujanjem | fluid flow cavitation |



**Autori**
Blaž Vajda[1], Zoran Žunič[2], Želimir Dobovišek[1], Breda Kegl[1]
[1]University of Maribor, Faculty of Mechanical Engineering,
Engine Research laboratory, Smetanova 17, SI-2000 Maribor, Slovenia
[2] AVL-AST d.o.o., Trg Leona Štuklja 5, SI-2000 Maribor, Slovenia

**Primljeno**
10.9.2010.

**Prihvaćeno**
06.05.2011.

**Blaž Vajda, Zoran Žunič, Želimir Dobovišek, Breda Kegl**

ISSN 0350-350X
GOMABN 50, 4, 335-360
Stručni rad/Professional paper
UDK 532.51 : .001.575 : .001.572 : 518.5 : 516.3 : 532.525 : 532.528

# INFLUENCE OF VARIOUS MESH TYPES ON CAVITATION PHENOMENA IN THE INJECTION NOZZLE

*Abstract*

*The evaporation of diesel fuel in the injection nozzle influences the injection characteristics and spray formation process significantly. In the presented paper the influence of various type of mesh on the cavitation phenomena is analysed. Since CPU (central processing unit) times are often high, partial models are used for the analysis. The numerical analysis is made for two types of fluid, diesel (D2) and biodiesel (B100), using computation fluid dynamic (CFD) program FIRE. The results are compared for various meshes and both types of fuel. The results show that higher pressure differences yield more cavitation in the injector nozzle holes and point out the importance of the structure of the mesh and its density.*

## Introduction

The development of the modern compression ignition engine is mainly connected with rising of injection pressure and the possibility of the injecting several jets during the single injection cycle. Both modifications influence positively the engine characteristics and the emission formation processes. On the other side rising of the injection pressure results in higher flow velocities in the nozzle hole channels and in evaporation of fuel in the nozzle holes. The fuel evaporates on the sharp edge at the nozzle inlet, where the static pressure falls below the fuel vapour pressure. The vapour is spreading along the nozzle hole and could also reach the outlet. The evaporation of fuel and cavitation process in the nozzle hole significantly influence the in-nozzle flow and spray formation process and it could also cause the erosion of nozzle material when bubbles collapse close to the nozzle wall. Since the typical diameter of the diesel injection nozzle is usually less than 1 mm and the pressure difference could even exceed the 200 MPa, the experimental analyses are quite difficult and limited. The majority of the experimental analysis on two phase flow in the injection nozzle used to be connected with the measurements and observation on the scaled-up models.

At the other side computation fluids dynamics (CFD) packages gained on importance in recent years, since by using the three-dimensional analysis many parameters could be calculated at very single cell of the modelled nozzle. The main problem that occurs in the CFD analysis is the required computation time. To shorten the time needed for calculation of the single analysis, simplified models of the nozzle are used.

## Nozzle gometry

Analyses were made for one-hole nozzle with sac volume and sharp edges at the nozzle hole inlet side. Dimension of the tested nozzle are presented in table 1.

Table 1: Nozzle dimensions

| | |
|---|---|
| Nozzle hole diameter | 0.68 mm |
| Nozzle hole channel length | 1 mm |
| Sac chamber diameter | 1.5 mm |
| Needle seat diameter | 1.36 |
| Needle tip cone angle | 120° |
| Needle seat cone angle | 60° |
| Maximal needle lift | 0.30 mm |

## Numerical models

### Theoretical backgrounds

Numerical analyses were done by using the CFD program FIRE. Two-phase flow is calculated with the two-equation model, with a continuous liquid and disperse vapour phase. Mass conservation equation:

$$\frac{\partial \alpha_k \rho_k}{\partial t} + \nabla \cdot \rho_k \mathbf{v}_k = \sum_{l=1;l\neq k}^{N} \Gamma_{kl} \tag{1}$$

$\alpha_k$ is volume fraction of phase k, $v_k$ is phase k velocity, and $\Gamma_{kl}$ represents the interfacial mass exchange between phases k and l. The compatibility condition must be obtained:

$$\sum_{k=1}^{N} \alpha_k \tag{2}$$

Momentum conservation equation:

$$\frac{\partial \alpha_k \rho_k \mathbf{v}_k}{\partial t} + \nabla \cdot \rho_k \mathbf{v}_k \mathbf{v}_k = -\alpha_k \nabla p + \nabla \alpha_k \left(\tau_k + T_k^{'}\right) + \alpha_k \rho_k \mathbf{g} + \sum_{l=1;l\neq k}^{N} \mathbf{M}_{kl} + \mathbf{v}_k \sum_{l=1;l\neq k}^{N} \Gamma_{kl} \tag{3}$$

where *f* is the body force vector which comprises of gravity *g*; $M_{kl}$ represents the momentum interfacial interaction between phases k and l, and *p* is pressure.

Pressure is assumed identical for all phases. The phase k shear stress, $\tau_k$, equals:

$$\tau_k = \mu_k \left[ \left( \nabla v_k + \nabla v_k^t \right) - \frac{2}{3} \nabla \cdot v_k \right] \tag{4}$$

$\mu_k$ is molecular viscosity. Reynolds stress $T_k^t$ equals:

$$T_k^{'} = -\rho_k \overline{\nabla v_k^{'} v_k^{'}} = \mu_k^{'} \left[ \left( \nabla v_k + \nabla v_k^t \right) - \frac{2}{3} \nabla \cdot v_k \right] - \frac{2}{3} \nabla \cdot v_k I \tag{5}$$

Turbulent viscosity is modelled as:

$$\mu_k^{'} = \rho_k C_\mu \frac{k_k^2}{\varepsilon_k} \tag{6}$$

Since the analyses in the presented paper were made at the constant temperature the enthalpy conservation equation will not be described in the details here.

Turbulent kinetic energy (TKE) conservation equation:

$$\begin{aligned} &\frac{\partial \alpha_k \rho_k k_k}{\partial t} + \nabla \cdot \alpha_k \rho_k \mathbf{v}_k k_k = \\ &\nabla \cdot \alpha_k \left( \mu_k + \frac{\mu_k^{'}}{\sigma_k} \right) \nabla k_k + \alpha_k P_k + \alpha_k P_{B,k} - \alpha_k \rho_k \varepsilon_k + \sum_{l=1;l\neq k}^{N} K_{kl} + k_k \sum_{l=1;l\neq k}^{N} \Gamma_{kl} \end{aligned} \tag{7}$$

Turbulence dissipation equation (TED):

$$\begin{aligned} &\frac{\partial \alpha_k \rho_k \varepsilon_k}{\partial t} + \nabla \cdot \rho_k \mathbf{v}_k \varepsilon_k = \nabla \cdot \alpha_k \left( \mu_k + \frac{\mu_k^{'}}{\sigma_\varepsilon} \right) \nabla \varepsilon_k + \alpha_k C_1 P_k \frac{\varepsilon_k}{k_k} - \alpha_k C_2 \rho_k \frac{{}_k \varepsilon_k^2}{k_k} \\ &+ \alpha_k C_3 \max\left( P_{B,k}, 0 \right) \frac{\varepsilon_k}{k_k} - \alpha_k C_4 \rho_k \varepsilon_k \nabla \cdot \mathbf{v}_k + \sum_{l=1;l\neq k}^{N} D_{kl} + \varepsilon_k \sum_{l=1;l\neq k}^{N} \Gamma_{kl} \end{aligned} \tag{8}$$

In two-equation model several mass exchange terms could be introduced (According to the type of two-phase flow.). In the presented analysis the cavitation model is employed.

Mass exchange term is defined with the following equations:

$$\Gamma_c = \frac{1}{C_R} \sin g(\Delta p) \cdot 3.85 \cdot \frac{\rho_d}{\sqrt{\rho_c}} N'''^{1/3} \alpha_d^{2/3} |\Delta p|^{1/2} \tag{9}$$

$$\Gamma_d = \sin g(\Delta p) \cdot 3.85 \cdot \frac{\rho_d}{\sqrt{\rho_c}} N'''^{1/3} \alpha_d^{2/3} |\Delta p|^{1/2} \tag{10}$$

Where the effective pressure difference equals:

$$\Delta p = p_{sat} - (p - C_E \frac{2}{3} \rho_c k_c) \tag{11}$$

$C_E$ is the Egler coefficient, which varies between 1 and 1.4. $C_{CR}$ is the condensation reduction factor. $N'''$ is the bubble number density, which is calculated assuming diminishing linear ramp:

$$N''' = \begin{cases} N_0''' & \alpha_d \le 0{,}5 \\ 2(N_0''') & \alpha_d > 0.5 \end{cases} \tag{12}$$

where $N_0'''$ represent the initial value of the bubble number density.
Interfacial momentum exchange term is defined with:

$$M_C = C_D \frac{1}{8} \rho_C A_i''' |v_r| v_r + C_{TD} \rho_c k_c \nabla \alpha_d = -M_d \tag{13}$$

where $v_r$ is the relative velocity and $A_i'''$ is the interfacial area density for bubbly flow:

$$A_i''' = \pi D_b^2 N''' = (36\pi)^{1/3} \alpha_d^{2/3} \tag{14}$$

$C_D$ is the discharge coefficient:

$$C_D = \begin{cases} \frac{24}{\mathrm{Re}_d} \cdot \left(1 + 0{,}15\,\mathrm{Re}_d^{0{,}687}\right) \Leftarrow \mathrm{Re}_d < 10^3 \\ 0{,}44 \Leftarrow \mathrm{Re}_d \ge 10^3 \end{cases} \tag{15}$$

$C_{TD}$ is turbulent dispersion coefficient, which value is between 0.05 and 0.5.

## Computation model

To analyse the flow characteristics of the in-nozzle flow different nozzle models were made. Since some analyses showed, that the pressure drop in nozzle is significant only in the area of the needle seat, sac chamber and nozzle holes, the meshes were modelled only for the above mentioned parts. For the maximal needle lift of 0.30 mm, two different nozzle models, representing real size and one half of the nozzle were made. First analyses show no significant changes between the results of the real size and one half model. For this reason we used one half model in further research.

## Initial and boundary conditions

According to steady state analysing conditions, pressure boundary conditions at the in- and outlet are specified. The fluids used for analysis are the diesel D2 and biodiesel B100, with the temperature of 293,15 K, the density 825 kg/m$^3$ for D2 and 875 kg/m$^3$ for B100 and dynamic viscosity of 2.45E-03 Ns/m$^2$ for D2 and 2.65E-03 Ns/m$^2$ for B100. K-ε model is employed. Since maximal velocities of used fuel are much smaller than the speed of sound, the fluid is assumed as incompressible.

## Used types of meshes and their various density

Numerical analysis includes various densities and types of meshes. Densities and their related type of used meshes are presented in table 1 and in figure 1. Standard approach is to use block-structured types of meshes, while we had a chance to compare (time) it with structured, to study the differences between them.

Table 1: Various densities and related types of meshes

| Name | Number of used elements | Mesh type | Physical model |
|---|---|---|---|
| mesh 1 | 21.440 | block-structured | single phase |
| mesh 2 | 41.920 | block-structured | single phase |
| mesh 3 | 162.050 | block-structured | single phase |
| mesh 4 | 22.880 | block-structured | two-phase |
| mesh 5 | 44.320 | block-structured | two-phase |
| mesh 6 | 183.040 | block-structured | two-phase |
| mesh 7 | 254.120 | block-structured | two-phase |
| mesh 8 | 22.900 | structured | two-phase |
| mesh 9 | 42.300 | structured | two-phase |
| mesh 10 | 46.540 | structured | two-phase |
| mesh 11 | 145.890 | structured | two-phase |
| mesh 12 | 175.050 | structured | two-phase |
| mesh 13 | 260.550 | structured | two-phase |

## Results

Results were taken on four different positions on the injector hole. The positions are presented in the figure 2. Position 1 is at the outlet, position 2 at the inlet of the nozzle and position 3 in in the middle of positions 1 and 2. The position 4 is along the nozzle. All the results were taken at the same time (1.765E-03 s). It is assumed that the needle is fully opened at this time.

### Results of the numerical analysis

Velocity profiles and volume fraction distributions derived from the CFD analyses for differently meshed models are presented in following figures. Figures 3 and 4 (left: back view; right: front view) show the results of volume fraction distribution in nozzle hole with various mesh densities.

The velocity profiles and volume fraction distributions in nozzle holes with various densities, figures 3 and 4 are almost identical. The results indicate already known fact that the outflow velocity is higher at holes with smaller inclination angles, what results in higher flow coefficient at those holes.

The results of the numerical analysis for velocity profiles, relative pressure and volume fraction on block-structured meshes of various densities are presented in figures 6 and 7 for single phase and on figures from 8 to 12 two-phase flow.

Figure 5 show the velocity profiles for block-structured type of mesh for single phase (B100). The results show no significant difference between the various densities. The differences are about 2 %. On the other side when we compare the result for velocity profile in position 4 (figure 6), the differences are about 5 %. The values for mesh with higher density are lower than the values for lower densities. The cause for this could be the appearance of cavitation.

Figure 7 show the results for relative pressure for single phase (only B100). It can be observed that there are now significant differences between various types of meshes. The difference between meshes with lower densities is less than 0.5%. In case when we compare the results for higher and lower densities the differences are about 10%.

The velocity profiles and volume fraction distribution at the nozzle inlet are almost identical (figures 8, 9 and 10). Comparison of the results in figures 11 and 13 show how different type of mesh significantly influences the velocity profiles. When we use structured (figure 11) mesh the velocity profiles are rougher then in case of block-structured (figure 13). When we compare the results for various density meshes there are difference between meshes with higher densities compared to meshes with lower density (figure 5-7 for single phase and figure 8-12 for two-phase model).

The vapour volume fraction results are presented in figure 8. Results for mesh 1 show the numerical failure caused by interpolation on insufficient number of elements (peak at length 6.5E-04 m). Peaks at length 5.5E-04 m for meshes 5 and 6 are caused by vapour cloud which is spreading through the hole till it reaches the outlet.

The results of influence of different type of fluid (D2 and B100) in nozzle showed no significant difference. Velocity field, velocity profiles and volume fraction distributions on the outlet are comparable. The results are comparable because the density of used fluids is similar and not so much different (difference is about 50 kg/m$^3$). The difference between dynamic viscosities is also very small and has no effect on the results. Values for mass-flow and viscosity were different (taken from experiment), while pressure and temperature were the same for both fuels.

The differences presented in figures 14-16 are very small. Some volume fraction (indicator for cavitation) analyses were made for different fuels and the difference is even smaller, so it cannot be presented properly in form similar as in figures 3 and 4.

As already stated the results of the analysis on the real size and one-half model of the nozzle showed no significant difference. Velocity fields, velocity profiles on the outlet and pressure distributions are comparable. This fact is shown on figure 17.

The difference in velocity in case of mesh 3 – ½ model and mesh 3 – real size model is maximum 1 % (figure 18). The calculated values of the flow coefficient are 0.678 for real size and 0.679 for half model, where the CPU times for one half model are only 43.5 % of the CPU needed for the real size model calculation. The pressure distributions presented in figure 18 show the very low pressure area in the re-circulation zone. This means, that the velocity at the outlet is higher and it is also more uniform. Higher output velocities result also in better atomisation of injected fuel. The vapour fraction for different types of fluid is presented in figure 19. When comparing the results the following could be observed. The structure of the cavitation is not dependent on the length of the nozzle hole. The shape of cavitation in the first part of the hole is almost identical. Later on the vapour cloud is spreading through the hole till it reaches the outlet.

## Conclusions

Considering above-mentioned results the following conclusions could be made:

- the numerical analysis show that higher pressure differences yield more cavitation,
- the results of the numerical analysis show that the block-structured type of mesh is better for numerical analysis in nozzle holes,
- comparison between structured and block-structured meshes show, that the velocity profiles are much rougher with structured mesh than in case of block-structured meshes,
- it is recommended to use meshes with higher density (higher than 100.000 elements) in case of in-nozzle flows, but meshes with lower density (between 20.000 and 100.000 ) can also be used for fast estimations,
- the results of numerical analysis for different types of fluids (D2 and B100) are comparable, however we recommend more simulations with additional parameters (pressure, temperature…) to be made,
- first analyses show no significant influence of the nozzle hole length on the shape of the cavitation.

**References**

[1] T. Yoda, T. Tsuda, Inflence of injection Nozzle improvement on DI Diesel Engine, SAE paper 970356.
[2] Y. Oishi et al., A computational Study into the Effect of the Injection Nozzle Inclintion Angle on the Flow Characteristics in Nozzle Holes, SAE paper 920580.
[3] C. Arcoumanis et. al., Analysis of the Flow in the Nozzle of a Vertical Multi Hole Diesel Engine Injector, SAE paper 980811.
[4] M. Kato et al., Flow Analysis in Nozzle Hole in Consideration of Cavitation, SAE paper 970052.
[5] Y. Oishi et al., A Computational Study into the Effects of the Injection Nozzle Inclination Angle on the Flow Characteristics in the Nozzle Holes, SAE paper 920580.
[6] K. Melcher, J. Chomiak, Experimentelle Untersuchung der Stroemung durch Dieseleinspritzduesen in stationaer betriebenen Grossmodel, Bosch Techn. Berichte 5 (1976) 4.
[7] ISO-4113:1988, Road Vehicles - Calibration Fluid Diesel Injection Equipment.
[8] H. Hardenberg, Die Nadelhubabhaengigkeit der Durchflussbeiwerte von Lochduessen fuer Direkteinspritzdieselmotoren, MTZ 46 (1985) 4, p. 143-146.
[9] FIRE Version 9 – Users manual, Multiphase Flow, AVL, 2009.
[10] L. C. Ganippa et al., The structure of cavitation and its effect on the spray pattern in a single hole diesel nozzle, SAE paper 2001-01-2008.
[11] L. C. Ganippa et al., Comparison of cavitation phenomena in transparent scaled-up single hole diesel nozzles, 4th International Symposium on Cavitation, California Institute of Technology, Pasadena, 2001.
[12] B. Göschel, Einspritzdüsenverschleiß, Forschungvereinigung Verbrenungskraftmachinen e.V., Heft R245, 1974.
[13] Kavitation. Abschlüßbericht über die Ergebnise des Schwerpunktprogramm 1966-1972, Deutsche Forschungsgemeinschafts, Boppard, 1974.
[14] G. König et al., Analysis of flow and cavitation phenomena in diesel injection nozzles and its effects on spray and mixture formation, 5. Internationales Symposium für Verbrennungsdiagnostik der AVL Deutschland, 6.-7. Juni, Baden Baden, 2002
[15] C. Arcoumanis et al., Visualisation of cavitation in diesel engine injectors, Mec. Ind. (2001) 2, 375-381.
[16] C. Arcoumanis et al., Investigation of cavitation in a vertical multi-hole injector, SAE paper 1999-01-0524.
[17] C. Arcoumanis et al, Cavitation in real-size multi-hole diesel injector nozzles, SAE paper 2000-01-1249.
[18] C. Badock et al, Investigation of cavitation in real size diesel injection nozzle, International Journal of Heat and Fluid Flow 20 (1999).

[19] K. Jung et.al., The breakup characteristics of liquid sheets formed by like-doublet injectors, Journal of Propulsion and Power (sent), http://rpl.snu.ac.kr/.

| UDK | ključne riječi | key words |
|---|---|---|
| 532.51 | numerički model dinamike fluida | computational fluid dynamics CDFmodel |
| .001.575. | gledište ispitivanja na materijalnom modelu | real model investigation viewpoint |
| .001.572 | gledište ispitivanja na teorijskom modelu | theoretical model investigation viewpoint |
| 518.5 | numeričko i grafičko modeliranje procesa | numeric and graphic process modeling |
| 516.3 | mrežni sistem prostornih koordinata | mesh system of space coordinates |
| 532.525 | istjecanje iz sapnica | fluid flow through nozzles |
| 532.528 | kavitacija strujanjem | fluid flow cavitation |

**Authors**
Blaž Vajda[1], Zoran Žunič[2], Želimir Dobovišek[1], Breda Kegl[1]
[1]University of Maribor, Faculty of Mechanical Engineering,
Engine Research Laboratory,
Smetanova 17, SI-2000 Maribor, Slovenia
[2] AVL-AST d.o.o.,
Trg Leona Štuklja 5, SI-2000 Maribor, Slovenia

**Received**
10.9.2010.

**Accepted**
06.05.2011.

**SLIKE / FIGURES**

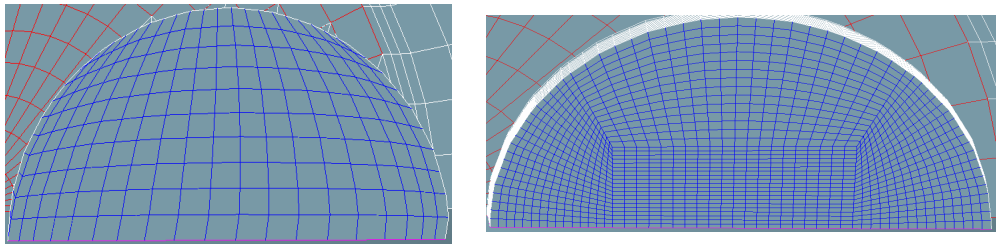

*A* *B*

Slika 1: Tipovi mreže mono (A) i više blokovna struktura (B)
Figure 1: Structured (A) and block-structured (B) types of used meshes

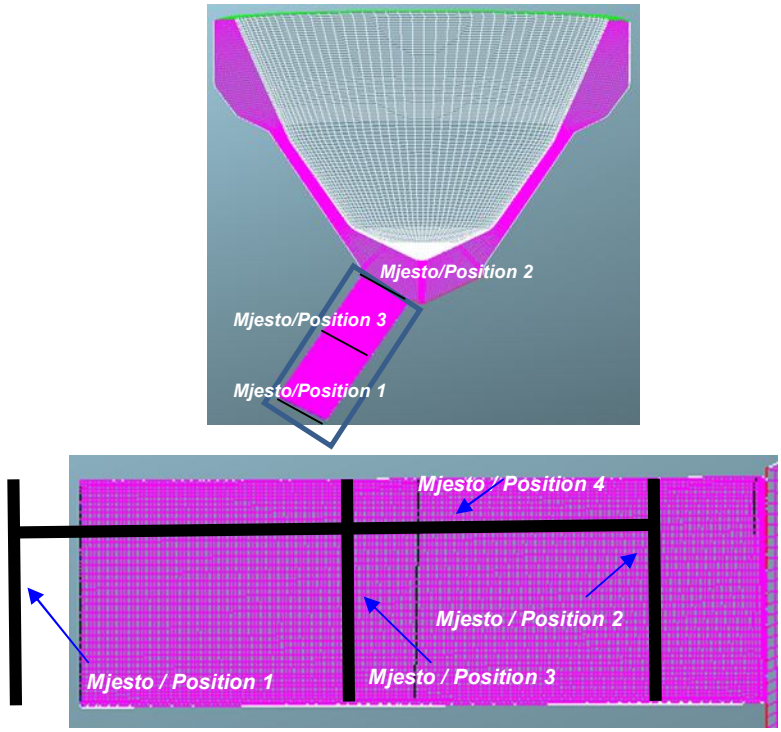


Slika 2: Položaji u točkama bilježenja rezultata
Figure 2: Positions of points were the results are taken

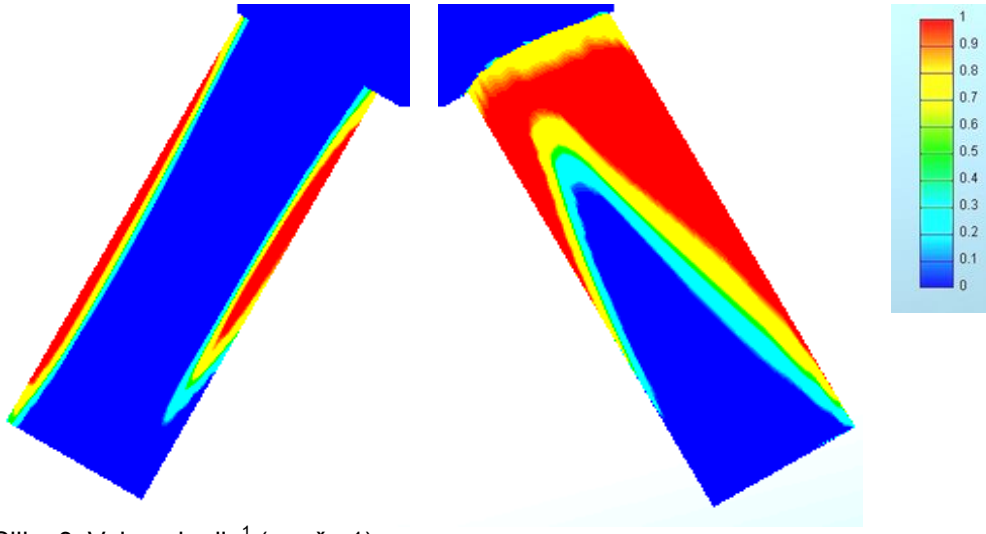


Slika 3: Volumni udio[1] (mreža 1)
Figure 3: Volume fraction[2] (mesh 1)

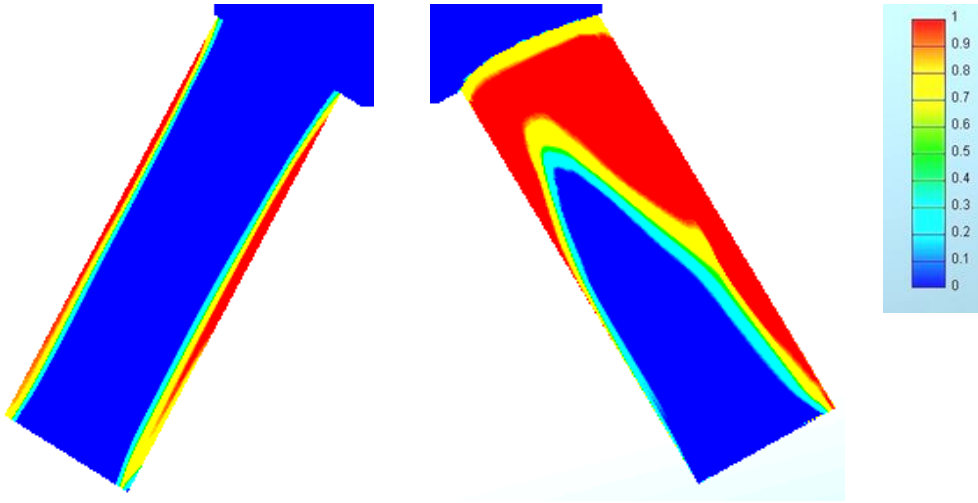


Slika 4: Volumni udio [3] (mreža 2)
Figure 4: Volume fraction[4] (mesh 2)

[1] udio parne faze u kapljevini
[2] vapour content in fluid
[3] udio parne faze u kapljevini
[4] vapour content in fluid

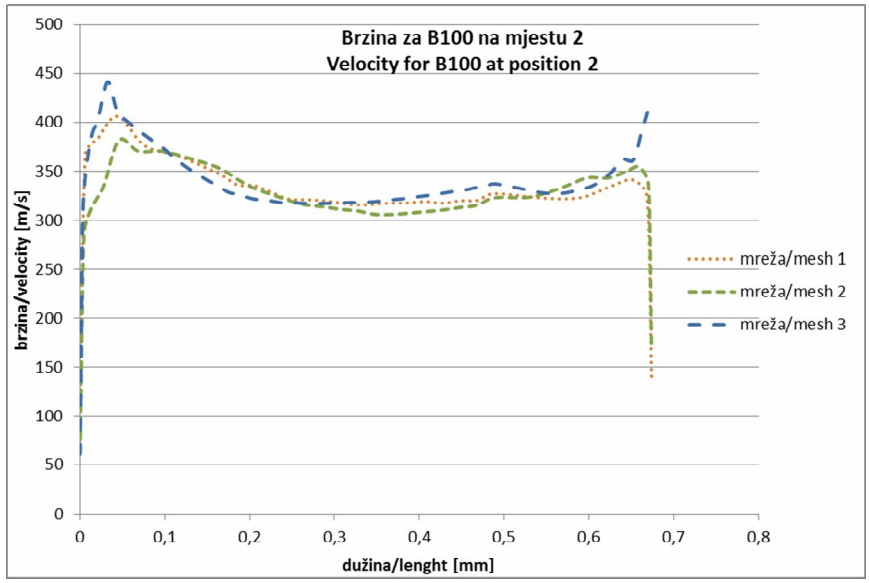


Slika 5: Profili brzine na mjestu 2 za blokovne strukture mreže i razne gustoće (jednofazni tok goriva) / Figure 5: Velocity profiles for block-structured type and various densities of used meshes at position 2 (single phase)

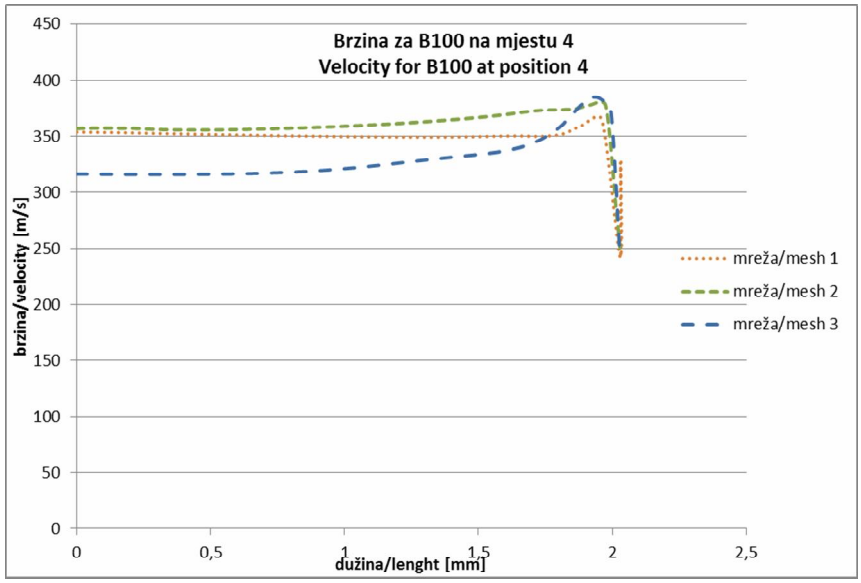


Slika 6: Profili brzine na mjestu 4 za blokovne strukture mreže i razne gustoće (jednofazni tok goriva) / Figure 6: Velocity profiles for block-structured type and various densities of used meshes at position 4 (single phase)

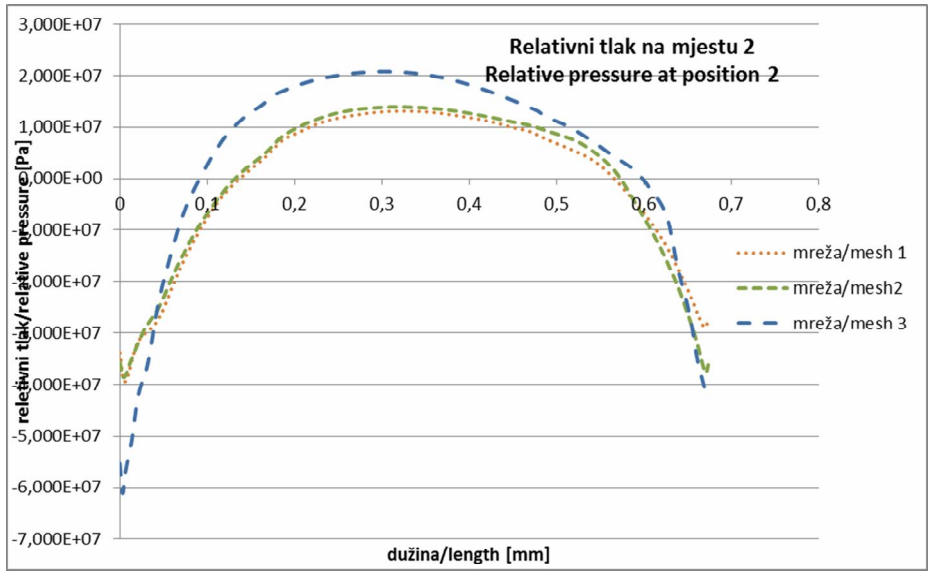


Slika 7: Relativni tlak na mjestu 2 za tipove mreže blokovne strukture i različite gustoće (jednofazni tok goriva) / Figure 7: Relative pressure for block-structured type and various densities of used meshes at position 2 (single phase)

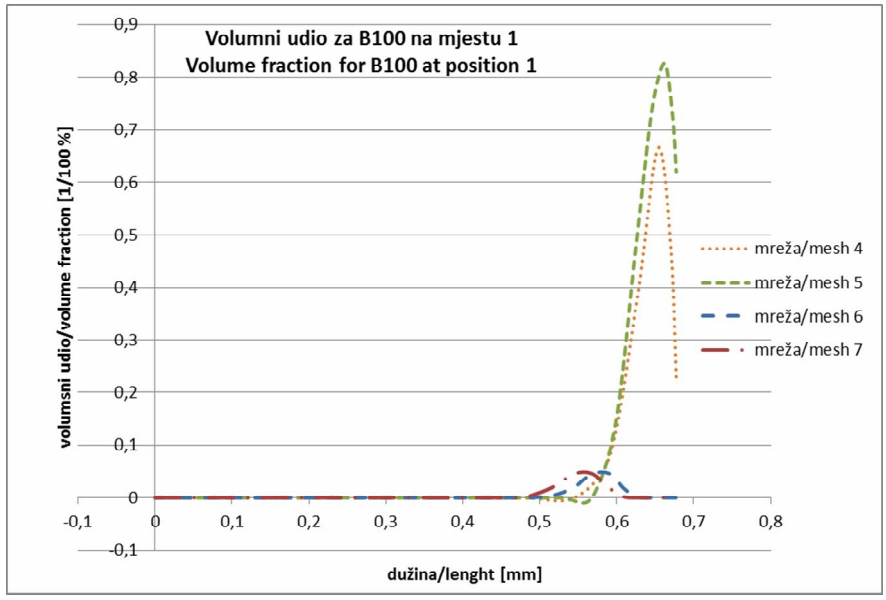


Slika 8: Volumni udio za mreže tipa blokovne strukture i različite gustoće na mjestu 1 (dvofazni tok goriva) / Figure 8: Volume fraction for block-structured type and various densities of used meshes at position 1 (two-phase)

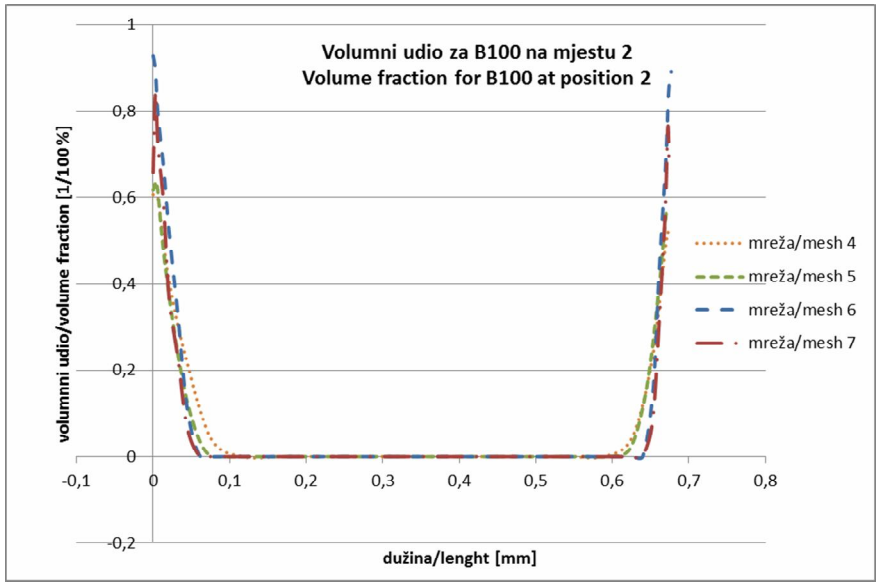


Slika 9: Volumni udio za mreže tipa blokovne strukture i različite gustoće na mjestu 2 (dvofazni tok goriva) / Figure 9: Volume fraction for block-structured type and various densities of used meshes at position 2 (two-phase)

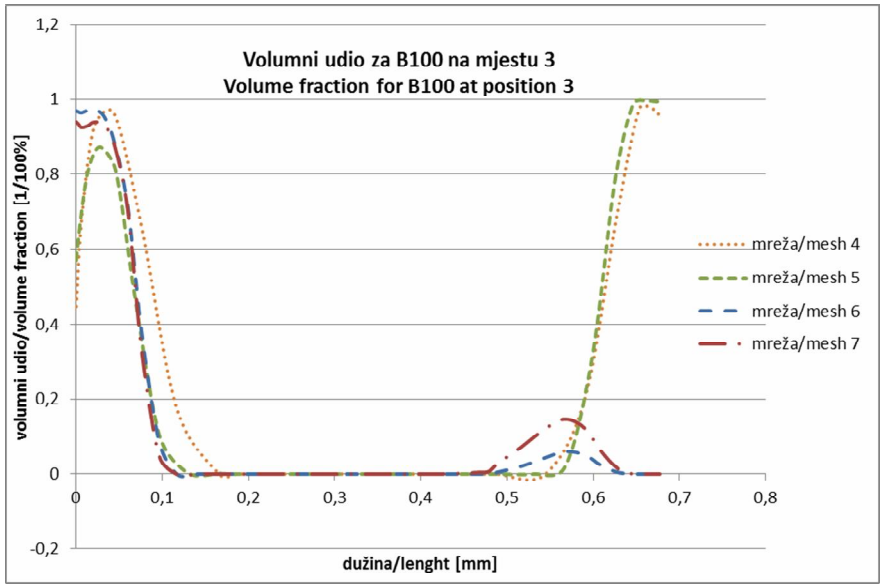


Slika 10: Volumni udio za mreže tipa blokovne strukture i različite gustoće na mjestu 3 (dvofazni tok goriva) / Figure 10: Volume fraction for block-structured type and various densities of used meshes at position 3 (two-phase)

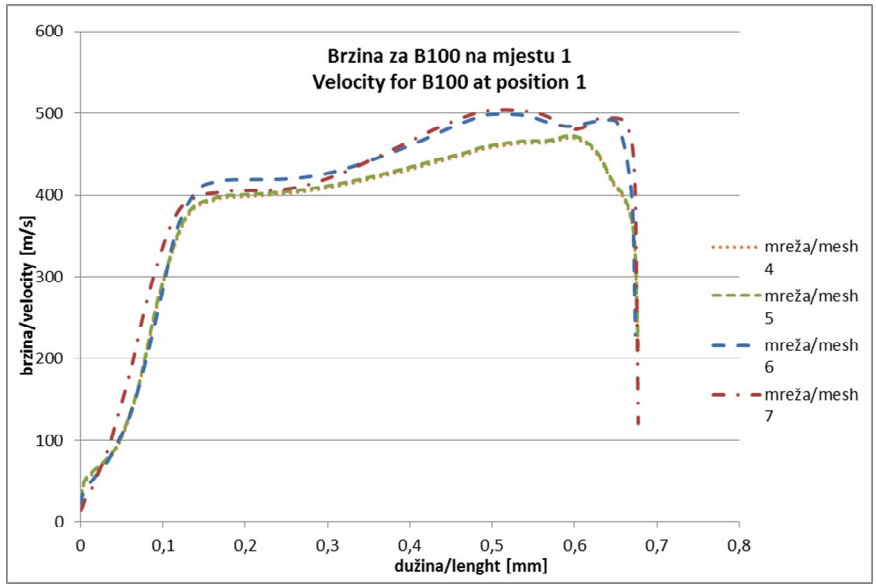


Slika 11: Profil brzine za mreže tipa blokovne strukture i različite gustoće na mjestu 1 (dvofazni tok goriva) / Figure 11: Velocity profiles for block-structured type and various densities of used meshes at position 1 (two-phase)

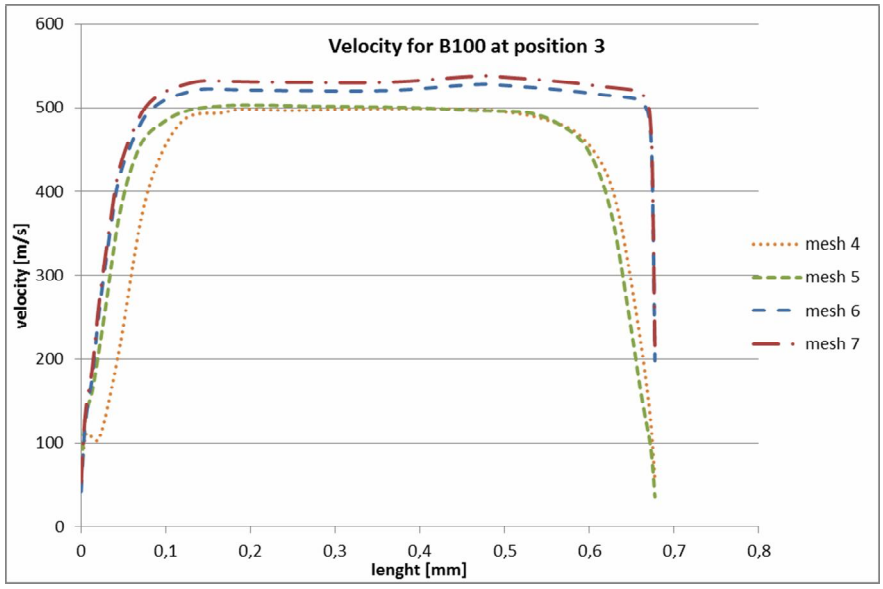


Slika 12: Profil brzine mreže tipa blokovne strukture i različite gustoće na mjestu 3 (dvofazni tok goriva) / Figure 12: Velocity profiles for block-structured type and various densities of used meshes at position 3 (two-phase)

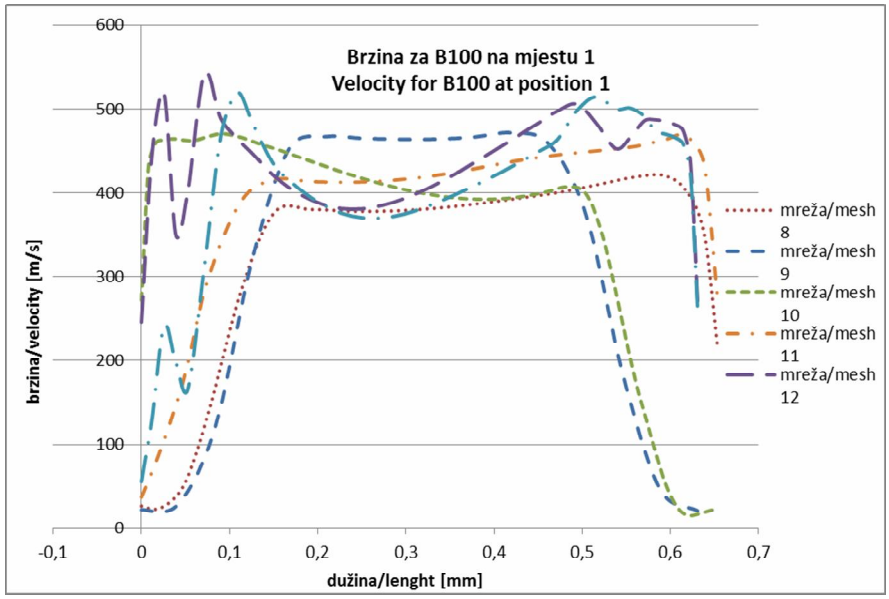


Slika 13: Profili brzine mreže jednostavne strukture različitih gustoća na mjestu 1
Figure 13: Velocity profiles for structured mesh and various densities of used meshes at position 1

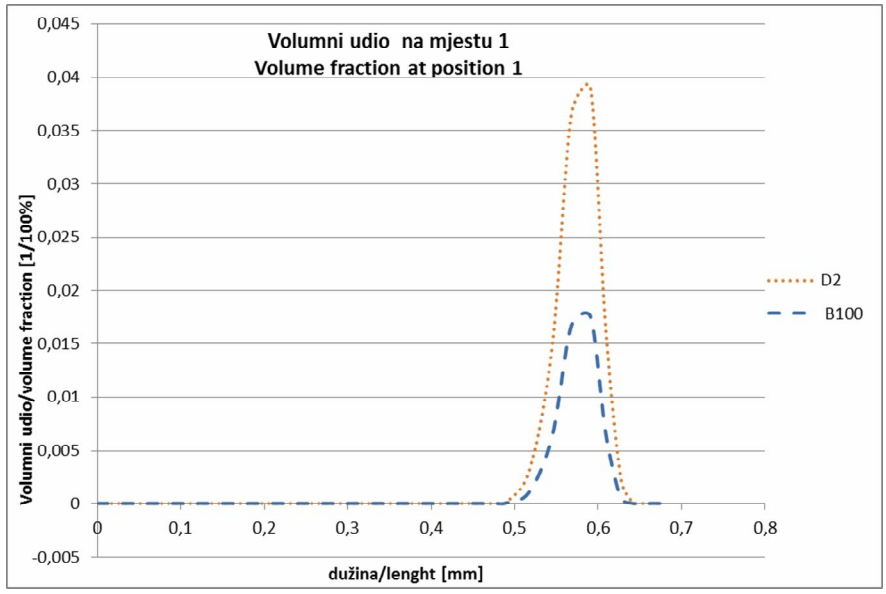


Slika 14: Volumni udio raznih vrsta fluida (D2 i B100) na mjestu 1 (mreže 6)
Figure 14: Volume fraction for different type of fluid (D2 and B100) at position 1 (mesh 6)

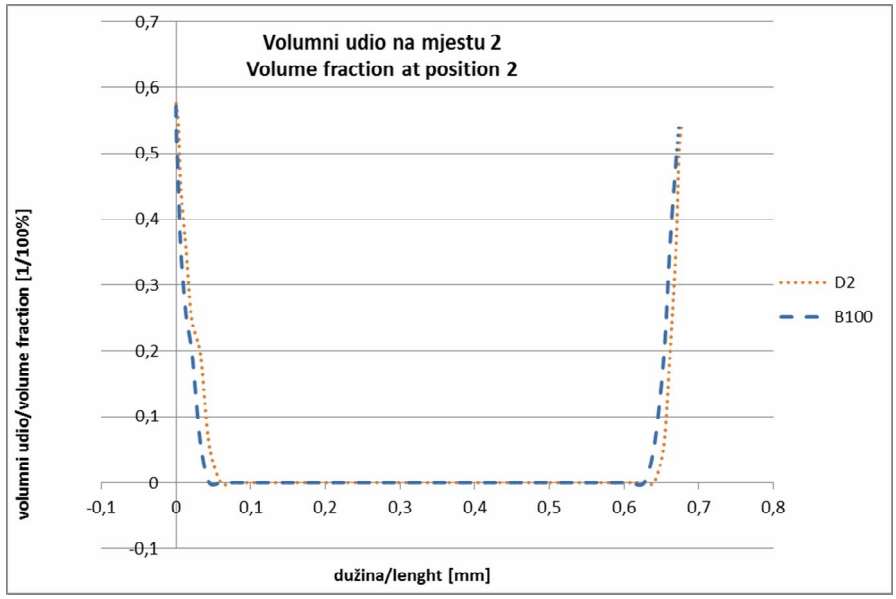


Slika 15: Volumni udio raznih vrsta fluida (D2 i B100) na mjestu 2 (mreže 6)
Figure 15: Volume fraction for different type of fluid (D2 and B100) at position 2 (mesh 6)

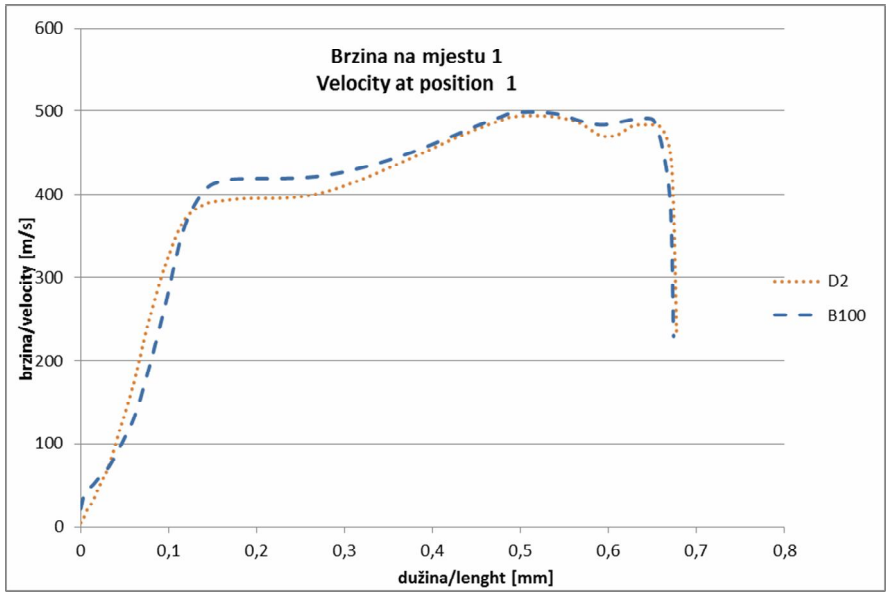


Slika 16: Profil brzine mase za fluide (D2 i B100) na mjestu 1 (mreže 6)
Figure 16: Velocity profiles for different type of fluid (D2 and B100) at position 1 (mesh 6)

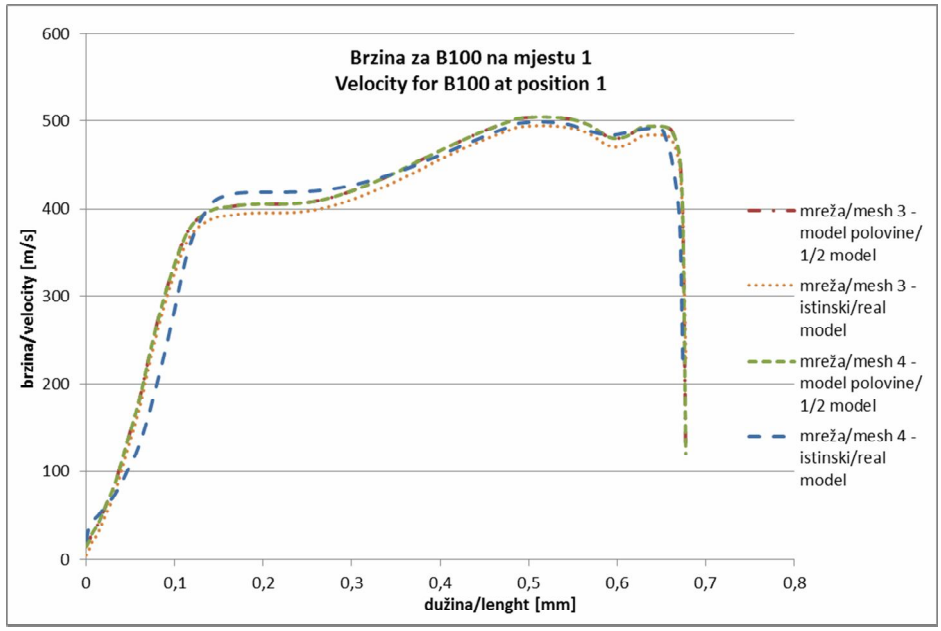


Slika 17: Profil brzina za tipove blokove strukture i korištene modele na mjestu 1
Figure 17: Velocity profiles for block-structured type and used models at position 1

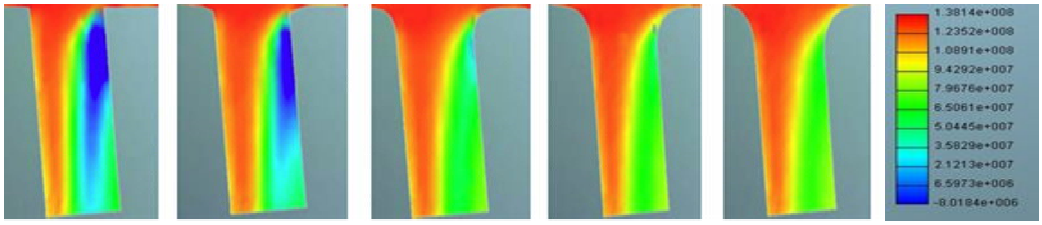

Slika 18: Podjela tlaka u provrtu sapnice (središnji rez, od lijeve: oštra ivica 0,05; 0,1; 0,15 i 0,2 mm, mjerilo: tamne boje-područje niskog tlaka, svijetle boje-područje visokog tlaka)
Figure 18: Pressure distribution in the nozzle hole (central cut, from left: sharp edge, 0.05, 0.1, 0.15 and 0.2 mm; scaling: dark colours-low pressure regions, light colours-high pressure)

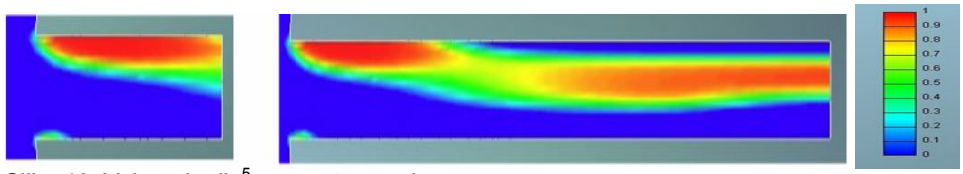

Slika 19: Volumni udio[5] u provrtu sapnice
Figure 19: Volume fraction[6] in nozzle hole

[5] udio parne faze u kapljevini
[6] vapour content in fluid